Cell Reports

Supplemental Information

Structural Basis for Molecular Discrimination by a 3',3'-cGAMP Sensing Riboswitch

Aiming Ren, Xin C. Wang, Colleen A. Kellenbeger, Kanagalaghatta R. Rajashankar, Roger Jones, Ming C. Hammond and Dinshaw J. Patel

Supplemental Table

Table S1. Crystallographic Statistics for 3', 3'-cGAMP Riboswitch with Bound 3', 3'-cGAMP and c-di-GMP, Related to Figure 1&3.

Crystal	**3', 3'-cGAMP complex**	**c-di-GMP complex**
Data collection	24-ID-C	24-ID-C
Space group	$P2_1$	C2
Cell dimensions		
a, *b*, *c* (Å)	66.5, 50.4, 78.4	174.8, 44.9, 68.2
α, β, γ (º)	90, 91.7, 90	90, 103.3, 90
Wavelength	0.9792	0.9792
Resolution (Å)	78.3-2.05 (2.16-2.05)	85.1-2.12 (2.24-2.12)
R_{merge}	0.051 (0.789)	0.044 (0.909)
$I/\sigma I$	13.5 (1.6)	16.3 (1.3)
Completeness (%)	98.3 (99.0)	98.1 (97.9)
Redundancy	3.3 (3.2)	3.3 (3.4)
Unique reflections	32313 (4741)	28937 (4171)
Refinement		
Resolution (Å)	42.5-2.0	85.1-2.12
No. reflections	29171	28916
R_{work}/R_{free}	0.21/0.25	0.22/0.25
No. atoms		
RNA	3606	3605
ligand	90	92
Cations	12	10
Water	196	48
B-factors		
RNA	34.0	69.5
ligand	26.6	52.2
Cations	52.7	77.6
Water	33.6	64.9
R.m.s deviations		
Bond lengths (Å)	0.013	0.027
Bond angles (º)	1.292	1.236

Values for the highest-resolution shell are in parentheses.

Table S2. ITC-based Binding Parameters for Complex Formation of 3', 3'-cGAMP Riboswitch with Added Cyclic Dinucleotides and G20A Mutant c-di-GMP Riboswitch with 3', 3'-cGAMP, Related to Figure 3&4.

3', 3'-cGAMP riboswitch				
Ligand	ΔH Kcal/mol	ΔS cal/mol/deg	N	Kd μM
3', 3'-cGAMP	- 25.1 ± 0.43	+ 54.6	0.57 ± 0.006	0.07 ± 0.02
c-di-GMP	- 5.0 ± 0.08	+ 10.5	1.62 ± 0.02	0.93 ± 0.15
c-di-AMP	--	--	--	--
2', 3'-cGAMP	--	--	--	--
2', 2'-cGAMP	--	--	--	--

G20A Mutant c-di-GMP Vc2 riboswitch				
Ligand	ΔH Kcal/mol	ΔS cal/mol/deg	N	Kd μM
3', 3'-cGAMP	- 22.3 ± 5.6	- 22.3	0.2 ± 0.04	1.45 ± 0.82

Table S3. Crystallographic Statistics for G20A Mutant c-di-GMP Vc2 Riboswitch with Bound 3', 3'-cGAMP, Related to Figure 4.

Crystal	**3', 3'-cGAMP complex**
Data collection	24-ID-C
Space group	$P2_1$
Cell dimensions	
a, *b*, *c* (Å)	51.7, 46.8, 80.8
α, β, γ (º)	90, 90.4, 90
Wavelength	0.9792
Resolution (Å)	46.8-2.08 (2.14-2.08)
R_{merge}	0.059 (0.679)
$I/\sigma I$	11.3 (0.6)
Completeness (%)	75.2 (42.2)
Redundancy	2.0 (1.2)
Unique reflections	17467 (763)
Refinement	
Resolution (Å)	43.7-2.08
No. reflections	17405
R_{work}/R_{free}	0.22/0.30
No. atoms	
RNA	1954
ligand	45
Cations	1
Water	11
B-factors	
RNA	53.8
ligand	64.0
Cations	74.2
Water	50.8
R.m.s deviations	
Bond lengths (Å)	0.012
Bond angles (º)	1.223

Values for the highest-resolution shell are in parentheses.

Table S4. Sequences of Riboswitch, Riboswitch-Spinach Constructs, and Primers, Related to Figure 1, 4&5.

Name	Sequence	Accession / Notes
Gm0970 (crystallography construct)	GGTATCGACAATACTAAACCATCCGCGAGGGTGGGACGGAAAGCCTAC AGGGTCTCTCTGAGACAGCCGGGATGCCAGAATATC	CP000148.1: 1079466-1079541
Gs1761 (crystallography construct)	GGTACACGACAATACTAAACCATCCGCGAGGATGGGGCGGAAAGCCTA AGGGTCTCCCTGAGACAGCCGGGCTGCCGAAATATC	AE017180.2 1922650-1922729; Red nt show U72C/C73U
Gm0970-Spinach	gacgcgactgaatgaaatggtgaaggacgggtccaATCGACAATACTAA ACCATCCGCGAGGGTGGGACGGAAAGCCTACAGGGTCT CTCTGAGACAGCCGGGATGCCGAATttgttgagtagagtgtgagctc cgtaactagtcgcgtc	CP000148.1: 1079466-1079541; Construct w/ red nt deleted used in Fig. S3 only
Gs1761-Spinach	gacgcgactgaatgaaatggtgaaggacgggtccaTACACGACAATACT AAACCATCCGCGAGGATGGGGCGGAAAGCCTAAGGGTC TCCCTGAGACAGCCGGGTCGCCGAAATAttgttgagtagagtgtg agctccgtaactagtcgcgtc	AE017180.2 1922650-1922729
Vc2-Spinach	gacgcgactgaatgaaatggtgaaggacgggtccaCACGCACAGGGCA AACCATTCGAAAGAGTGGGACGCAAAGCCTCCGGCCTAA ACCAGAAGACATGGTAGGTAGCGGGGTTACCGATGttgttga gtagagtgtgagctccgtaactagtcgcgtc	CP007634.1 1329924-1330010
Cc9469	gacgcgactgaatgaaatggtgaaggacgggtccaTCGATCAGCAAAAC TAGCGAAAGCTAGTGACGCAAAGCTACAGGGATTTCCCC TTTTAACAGGGATGTCAGCCAGCTGCAGGttgttgagtagagtgt gagctccgtaactagtcgcgtc	ADLJ01000004.1 176358-176439
Bc9140	gacgcgactgaatgaaatggtgaaggacgggtccaAATATTTTTAGCACA CTATTCGAAAGGATAGGCCGCAAAGCTTAGAGTCTACGG TAATATATTGGTTACTAAGATCGTCTGGTTGCACATTttgttga gtagagtgtgagctccgtaactagtcgcgtc	ACMP01000037.1 9235-9325
Ck2324	gacgcgactgaatgaaatggtgaaggacgggtccaTTGATAATAGCACA CTTATCGAAAGGTAGGGTCGCAAAGCTATGGGTCTTAAG AAAATTATTTTTCTATGATTGCCAGGTTGCCAAttgttgagtaga gtgtgagctccgtaactagtcgcgtc	CP000673.1 2377707-2377792
Gs2885b	gacgcgactgaatgaaatggtgaaggacgggtccaCGATAAGACTAAAC CGTCCGCGAGGGCGGGGCGGAAAGCCTAGGGTCTCCTA GAGACAGCCGGGATGCCGttgttgagtagagtgtgagctccgtaactagt cgcgtc	AE017180.1 3168890-3168959
Gu2327	gacgcgactgaatgaaatggtgaaggacgggtccaCGAAAATACTAAAC CATTCGCGAGAATGGGACGGAAAGCCTAAAGGGTCTCAC CGAGACAGCCGGGTCGCCGttgttgagtagagtgtgagctccgtaacta gtcgcgtc	CP000698.1 2691964-2692035
Gm2037	gacgcgactgaatgaaatggtgaaggacgggtccaCGACAATACTCAAC CATCCGTGAGGATGGGGCGGAAAGCCTATTGGGTCTCAC CGAGACAGCCGGGTTGCCGttgttgagtagagtgtgagctccgtaacta gtcgcgtc	CP000148.1 2280695-2280766
Gm0232	gacgcgactgaatgaaatggtgaaggacgggtccaCGACAATACTAAAC CATCCGCGAGGATGGGGCGGAAAGCCCATAGGGTCTCA CCGAGACAGCCGttgttgagtagagtgtgagctccgtaactagtcgcgtcGG TTGCCG	CP000148.1 264999-265062
Pp0574a-Spinach	gacgcgactgaatgaaatggtgaaggacgggtccaCACGATAATACTCA ACCATCCGCGAGGATGGGGCGGAAAGCCTACAGGGTCT CACCGAGACAGCCGGGTTGCCGAAATGttgttgagtagagtgtga	CP000482.1: 609390-609468

	gctccgtaactagtcgcgtc	
Pp2849-Spinach	gacgcgactgaatgaaatggtgaaggacgggtccaTAGACGACAATACTAAACCATTCGCGAGAATGGGACGGAAAGCCTACAGGGTCTCACCGAGACAGCCGGGTCGCCGAAATAttgttgagtagagtgtgagctccgtaactagtcgcgtc	CP000482.1: 3117926-3118006
Pp0574b-Spinach	gacgcgactgaatgaaatggtgaaggacgggtccaTAGACGATACTACTTAACCATTCGCAAGAATGGGGCGGAAAGCCTAAGGGTCTTACTGAGACAGCCGGGTTGCCGAAATAttgttgagtagagtgtgagctccgtaactagtcgcgtc	CP000482.1: 609610-609689
Pp2572-Spinach	gacgcgactgaatgaaatggtgaaggacgggtccaATCGATACTACTAAACCATCCGCGAGGATGGGACGGAAAGCCCACAGGGTCTCCAGAAGACAGCCGGGTCGCCGAAATttgttgagtagagtgtgagctccgtaactagtcgcgtc	CP000482.1: 2787032-2787109
Primer F	ccaagtaatacgactcactataGACGCGACTGAATGAAATGGTGAAGG	Extended T7 promoter (small caps)
Primer R	GACGCGACTAGTTACGGAGCTCACAC	

Table S5. Sequences of Mutant Riboswitch-Spinach Constructs, and Quikchange Primers, Related to Figure 5(provided as an Excel file).

Supplementary Figures

Figure S1. Chemical formula of cGAMP linkage isomers, omit maps of the binding pockets and ITC binding curves of 3',3'-cGAMP riboswitch with bound 3',3'-cGAMP and c-di-GMP and a structural comparison of 3',3'-cGAMP riboswitch and c-di-GMP riboswitch complexes, Related to Figure 1-4.

(A) Chemical formula of 3',3'-cGAMP, 2',3'-cGAMP and 2',2'-cGAMP.

(B) Omit electron density map (4σ) of 3',3'-cGAMP ligand in the binding pocket of the complex of 3',3'-cGAMP riboswitch with bound 3',3'-cGAMP.

(C) ITC-based study of the binding of 3',3'-cGAMP to the 3',3'-cGAMP riboswitch.

(D) ITC-based study of the binding of c-di-GMP to the 3',3'-cGAMP riboswitch.

(E) Omit electron density map (4σ) of the ligand c-di-GMP and pairing of Gα with A14 in the binding pocket of the complex of the 3',3'-cGAMP riboswitch with bound c-di-GMP.

(F) Superposition of structures of the binding pockets of the complexes of 3',3'-cGAMP riboswitch with bound 3',3'-cGAMP (in green) and bound c-di-GMP (in magenta). The bound ligands and the two key residues G42 and A14 are shown in stick.

(G) Superposition of the structures of the complexes of 3',3'-cGAMP riboswitch with bound 3',3'-cGAMP (in green) and c-di-GMP Vc2 riboswitch with bound c-di-GMP (in orange). The alignment was undertaking by superposing of stems P2 in the two complexes.

Figure S2. The P2a Region is Conserved in 3',3'-cGAMP Riboswitches, Related to Figure 5.

(A) Partial sequence alignment of GEMM-I riboswitch sequences that were found to selectively bind c-di-GMP, 3',3'-cGAMP, or be promiscuous for both (Kellenberger et. al. 2015). Except for Vc2, all sequences harbor an A at the nucleotide position predicted to interact with Aα or Gα of the ligand. The predicted base-pairs of the pairing stem P2 are denoted by < and >. The P2a region is highlighted in pink. Four sequences with conservation of this region from *Pelobacter propionicus* are shown. All full sequences are shown in Table S4.

(B) Spinach-based selectivity screen of the four *Pelobacter propionicus* GEMM-I riboswitches.

(C) Consensus sequence and secondary structure models for 3',3'-cGAMP (also called GEMM-Ib) riboswitches that harbor an A (left panel) or G (right panel) at the nucleotide position predicted to interact with Aα or Gα of the ligand. These models are based on functionally characterized sequences (28 and 4 representatives for left and right panels, respectively) from this study (Fig. S2B) and from Kellenberger et al. 2015. Consistent with other figures, the P2a region is indicated by pink boxes and the bulges in P3 are indicated by a blue box. The nucleotide position predicted to interact with Gβ of the ligand also is boxed.

Figure S3. The P2a Region Affects Ligand Selectivity of the Gs1761 3',3'-cGAMP Riboswitch, Related to Figure 5.

(A) Secondary structure of Gs1761, the 3',3'-cGAMP-selective riboswitch whose structure was elucidated by x-ray crystallography in this study. The P2a region is indicated by pink boxes. Green arrows indicate the positions in the P1 stem to which the Spinach aptamer was fused. The crystallography construct has the two blue nucleotides reversed (U72C, C73U).

(B) Spinach-based selectivity screen of wild-type Gs1761 riboswitch constructs with mutations to the P2a region shown. Fluorescence activation was measured in the presence of no ligand or different cyclic dinucleotides at the indicated concentrations. The nucleotides from Gs1761 (pink) were changed to those from the c-di-GMP-selective riboswitch, Vc2 (gray).

(C) Same as part (B) for the Gs1761 crystallography construct.

Figure S4. Changes to the Wobble Base Pair Alone Affects Ligand Selectivity and Corresponding Mutations to the Vc2 c-di-GMP Riboswitch Does Not Result in a 3',3'-cGAMP Selective Riboswitch, Related to Figure 5.

(A) Spinach-based selectivity screen of Gm0970 riboswitch constructs with mutations to the P2a region shown. Nucleotide colors indicate a match to the sequence from Gm0970 (pink), Vc2 (gray), or neither (white). The inset shows data for constructs

related to the first four shown in the main graph (see Methods, Table S4), except analyzed at higher RNA concentrations.

(B) Spinach-based selectivity screen of Vc2 riboswitch constructs with mutations to the P2a region shown. Fluorescence activation was measured in the presence of no ligand or different cyclic dinucleotides at the indicated concentrations. The nucleotides from Vc2 (gray) were changed to those from 3',3'-cGAMP-selective riboswitches (pink). The different nucleotide numbering schemes for Vc2 and Gs1761 are shown for comparison.

Figure S5. The P2a Stem and the Ligand Binding Pocket for the 3',3'-cGAMP Riboswitch, Related to Figure 1&5.

(A) A schematic depicting the proximity of the P2a stem to riboswitch nucleotides involved in stacking interactions (brown) and hydrogen-bonding (blue) to the cyclic dinucleotide ligand.

(B) Same view as in part A with inclusion of the stapling interaction between the P2a stem and A43 and showing A42.

(C) Chemical structures of different possible hydrogen-bonding modes for Gα versus Aα.

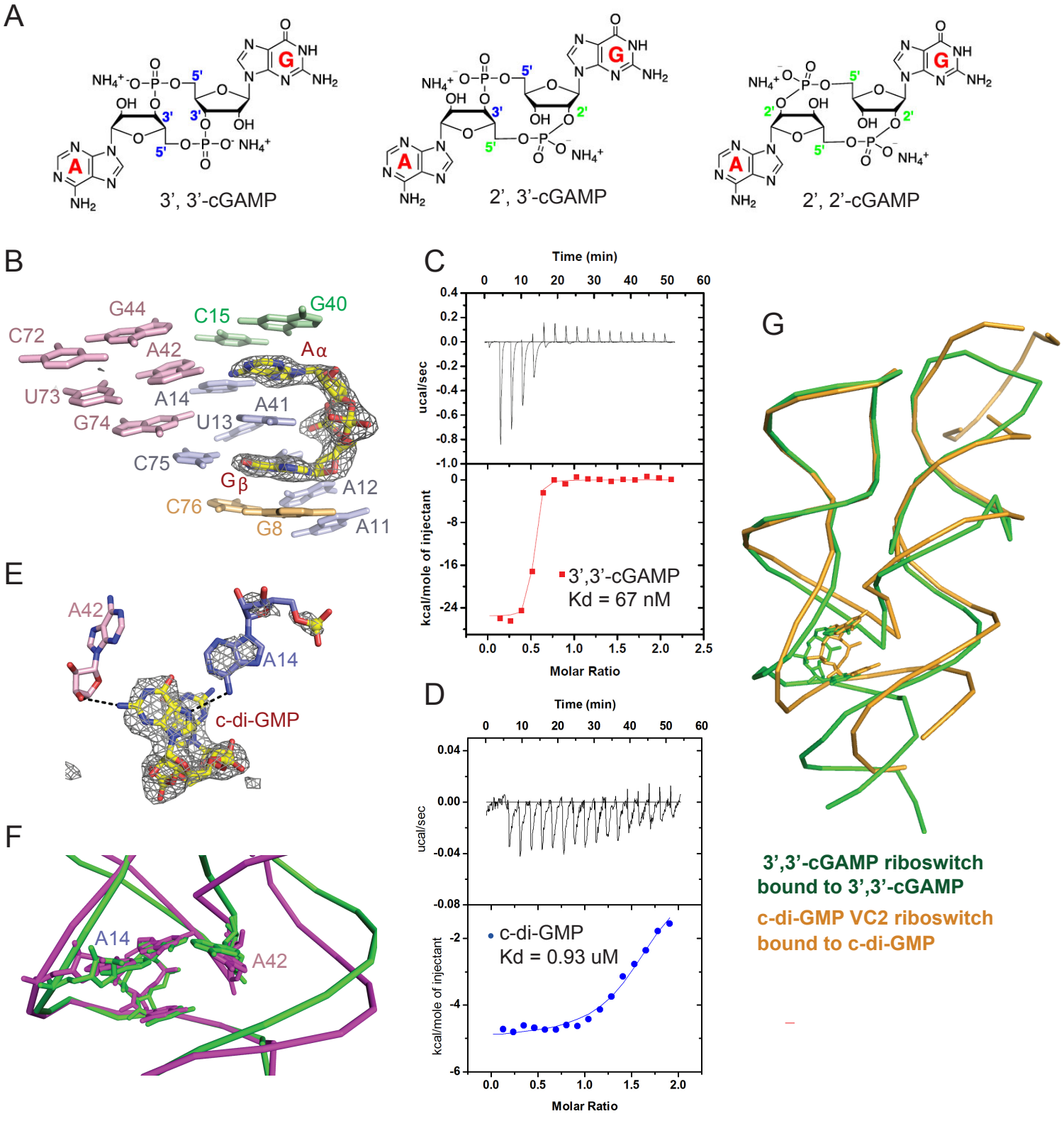
A
3', 3'-cGAMP
2', 3'-cGAMP
2', 2'-cGAMP
B
G44
C15
G40
C72
A42
Aα
U73
A14
A41
G74
U13
C75
Gβ
A12
C76
G8
A11
C
Time (min)
ucal/sec
kcal/mole of injectant
3',3'-cGAMP
Kd = 67 nM
Molar Ratio
D
Time (min)
ucal/sec
kcal/mole of injectant
c-di-GMP
Kd = 0.93 uM
Molar Ratio
E
A42
A14
c-di-GMP
F
A14
A42
G
3',3'-cGAMP riboswitch
bound to 3',3'-cGAMP
c-di-GMP VC2 riboswitch
bound to c-di-GMP

Fig. S1

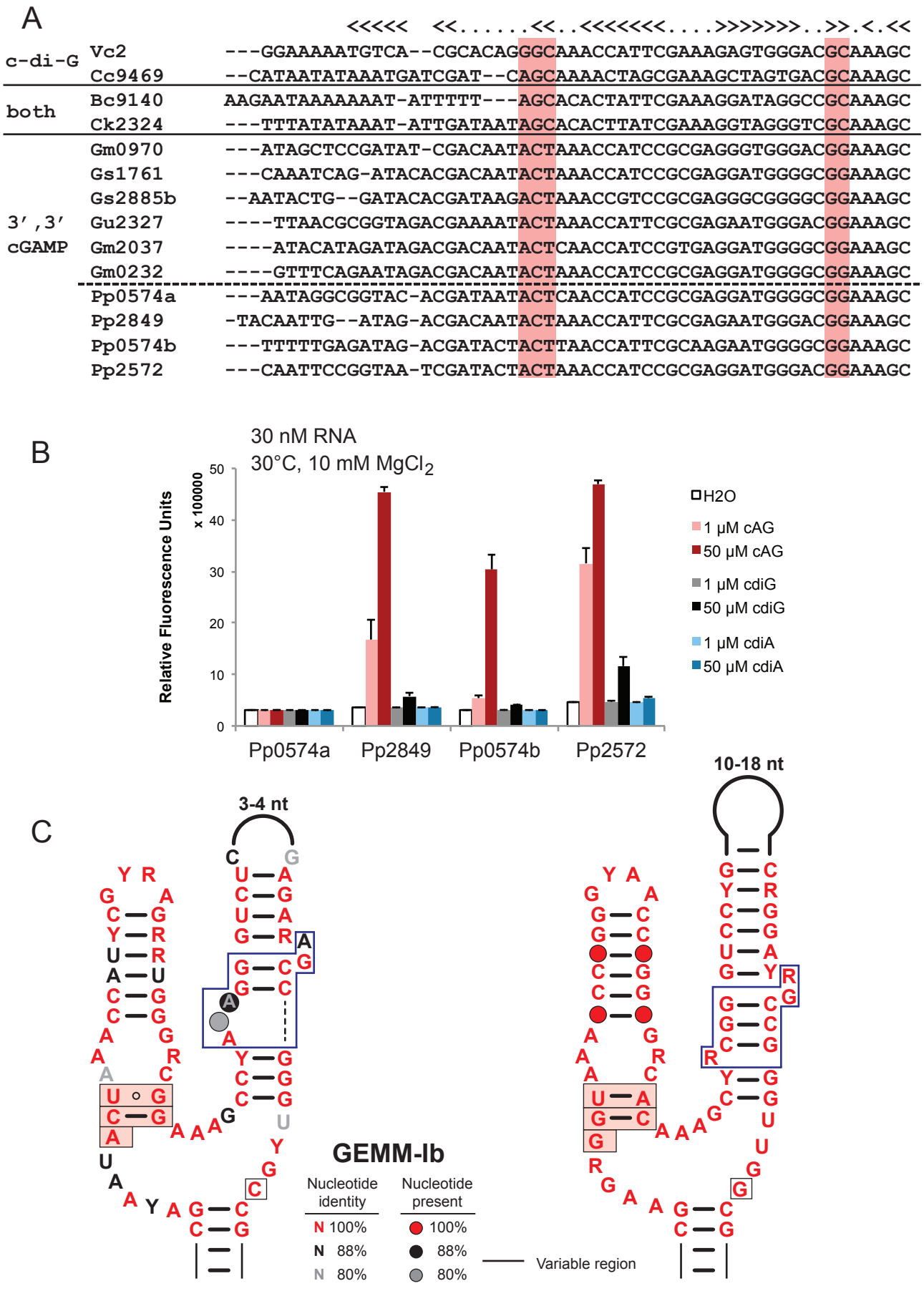
A
<<<<< <<.....<<..<<<<<<<....>>>>>>>..>>.<.<<
c-di-G
Vc2 ---GGAAAAATGTCA--CGCACAGGGCAAACCATTCGAAAGAGTGGGACGCAAAGC
Cc9469 --CATAATATAAATGATCGAT--CAGCAAAACTAGCGAAAGCTAGTGACGCAAAGC
both
Bc9140 AAGAATAAAAAAAT-ATTTTT---AGCACACTATTCGAAAGGATAGGCCGCAAAGC
Ck2324 ---TTTATATAAAT-ATTGATAATAGCACACTTATCGAAAGGTAGGGTCGCAAAGC
Gm0970 ---ATAGCTCCGATAT-CGACAATACTAAACCATCCGCGAGGGTGGGACGGAAAGC
Gs1761 ---CAAATCAG-ATACACGACAATACTAAACCATCCGCGAGGATGGGGCGGAAAGC
Gs2885b --AATACTG--GATACACGATAAGACTAAACCGTCCGCGAGGGCGGGGCGGAAAGC
3′,3′ Gu2327 ----TTAACGCGGTAGACGAAAATACTAAACCATTCGCGAGAATGGGACGGAAAGC
cGAMP Gm2037 ----ATACATAGATAGACGACAATACTCAACCATCCGTGAGGATGGGGCGGAAAGC
Gm0232 ----GTTTCAGAATAGACGACAATACTAAACCATCCGCGAGGATGGGGCGGAAAGC
Pp0574a ---AATAGGCGGTAC-ACGATAATACTCAACCATCCGCGAGGATGGGGCGGAAAGC
Pp2849 -TACAATTG--ATAG-ACGACAATACTAAACCATTCGCGAGAATGGGACGGAAAGC
Pp0574b ---TTTTTGAGATAG-ACGATACTACTTAACCATTCGCAAGAATGGGGCGGAAAGC
Pp2572 ---CAATTCCGGTAA-TCGATACTACTAAACCATCCGCGAGGATGGGACGGAAAGC
B
30 nM RNA
30°C, 10 mM MgCl2
Relative Fluorescence Units
x 100000
50
40
30
20
10
0
H2O
1 μM cAG
50 μM cAG
1 μM cdiG
50 μM cdiG
1 μM cdiA
50 μM cdiA
Pp0574a
Pp2849
Pp0574b
Pp2572
C
3-4 nt
10-18 nt
GEMM-Ib
Nucleotide identity
Nucleotide present
N 100%
N 88%
N 80%
100%
88%
80%
Variable region

Fig. S2

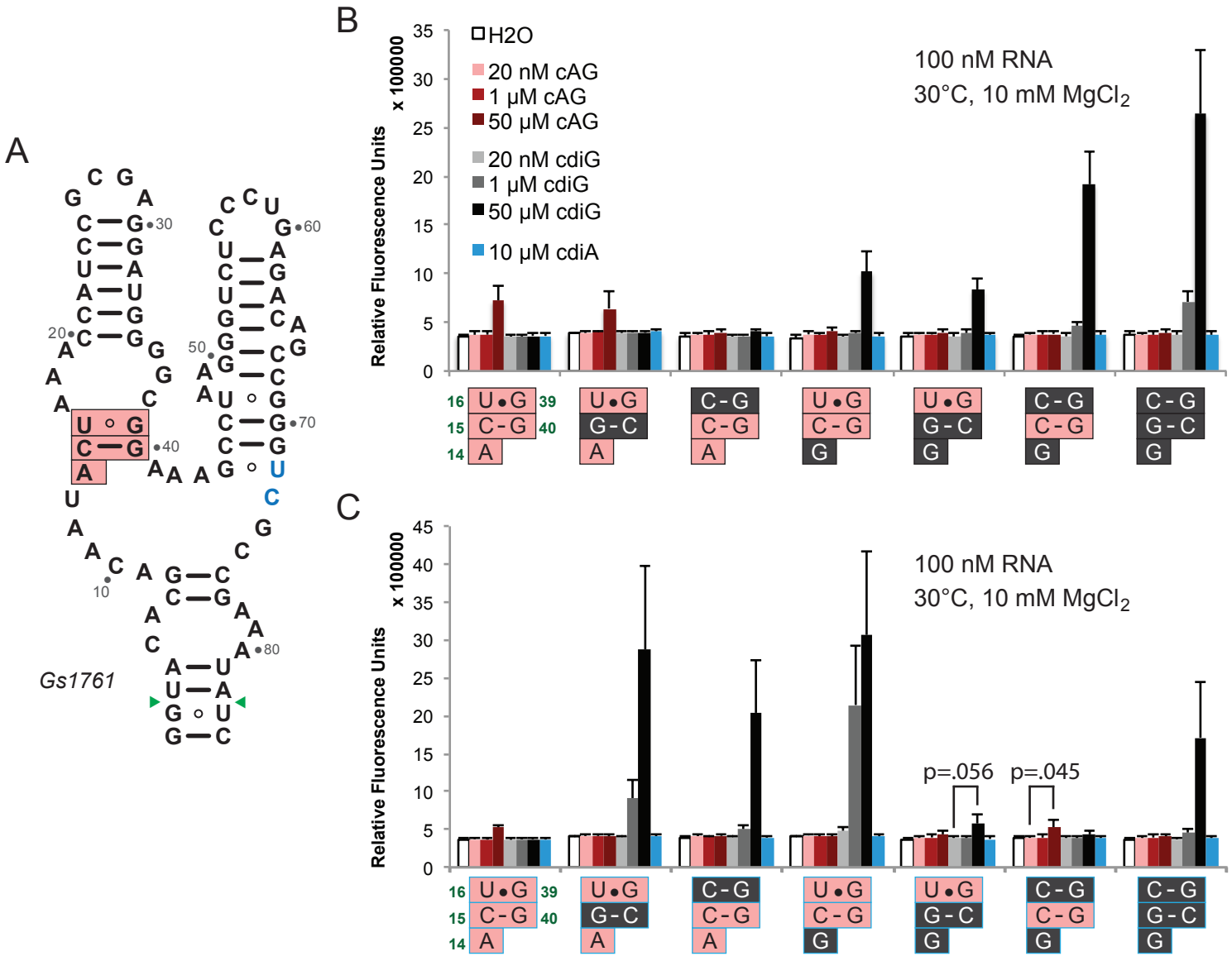
A
Gs1761
B
H2O
20 nM cAG
1 µM cAG
50 µM cAG
20 nM cdiG
1 µM cdiG
50 µM cdiG
10 µM cdiA
100 nM RNA
30°C, 10 mM MgCl2
Relative Fluorescence Units
x 100000
C
p=.056
p=.045

Fig. S3

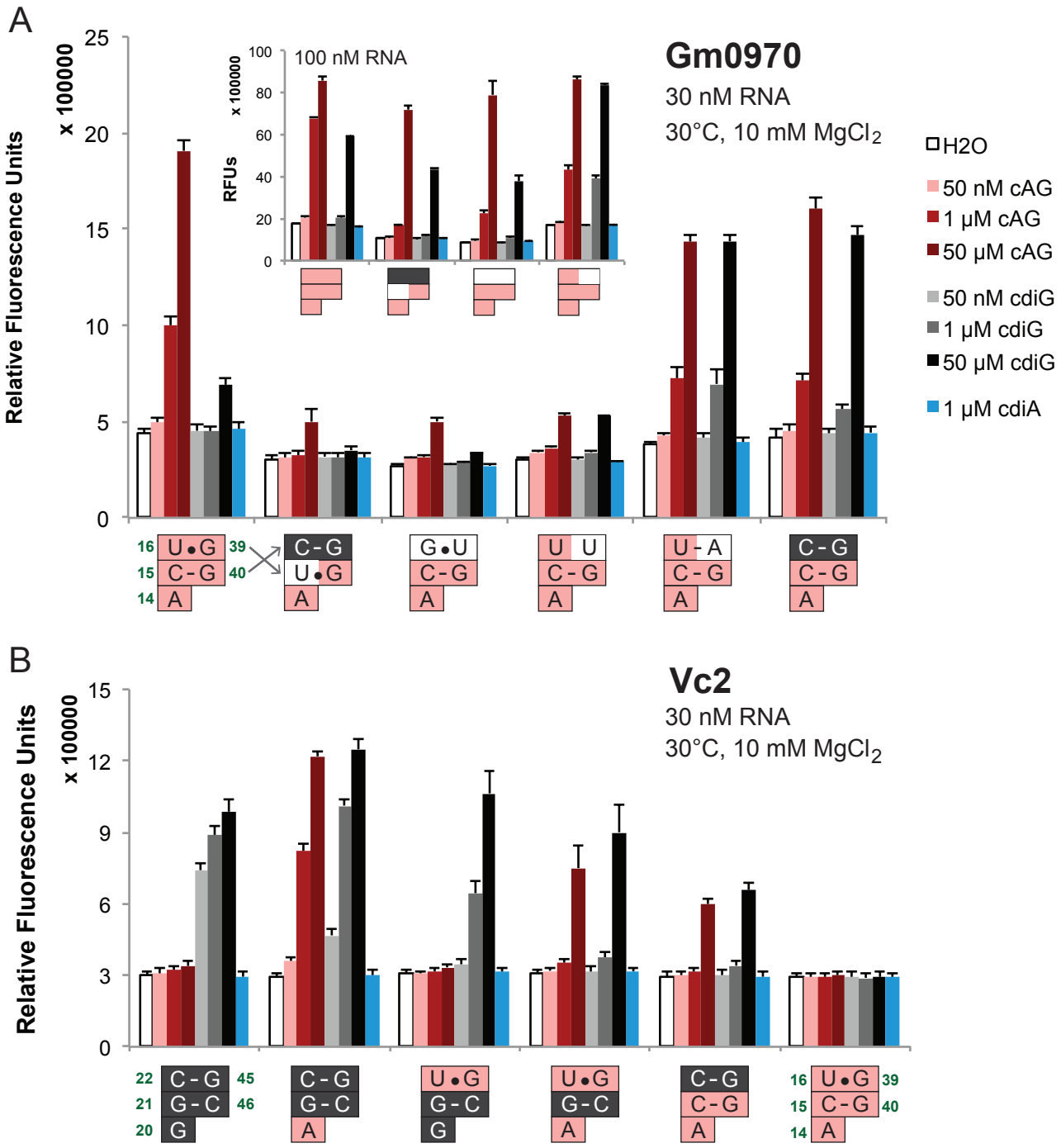
A
Relative Fluorescence Units
x 100000
25
20
15
10
5
0
100 nM RNA
RFUs
x 100000
100
80
60
40
20
0
Gm0970
30 nM RNA
30°C, 10 mM MgCl2
H2O
50 nM cAG
1 µM cAG
50 µM cAG
50 nM cdiG
1 µM cdiG
50 µM cdiG
1 µM cdiA
16 U•G 39
15 C-G 40
14 A
C-G
U•G
A
G•U
C-G
A
U U
C-G
A
U-A
C-G
A
C-G
C-G
A
B
Relative Fluorescence Units
x 100000
15
12
9
6
3
0
Vc2
30 nM RNA
30°C, 10 mM MgCl2
22 C-G 45
21 G-C 46
20 G
C-G
G-C
A
U•G
G-C
G
U•G
G-C
A
C-G
C-G
A
16 U•G 39
15 C-G 40
14 A

Fig. S4

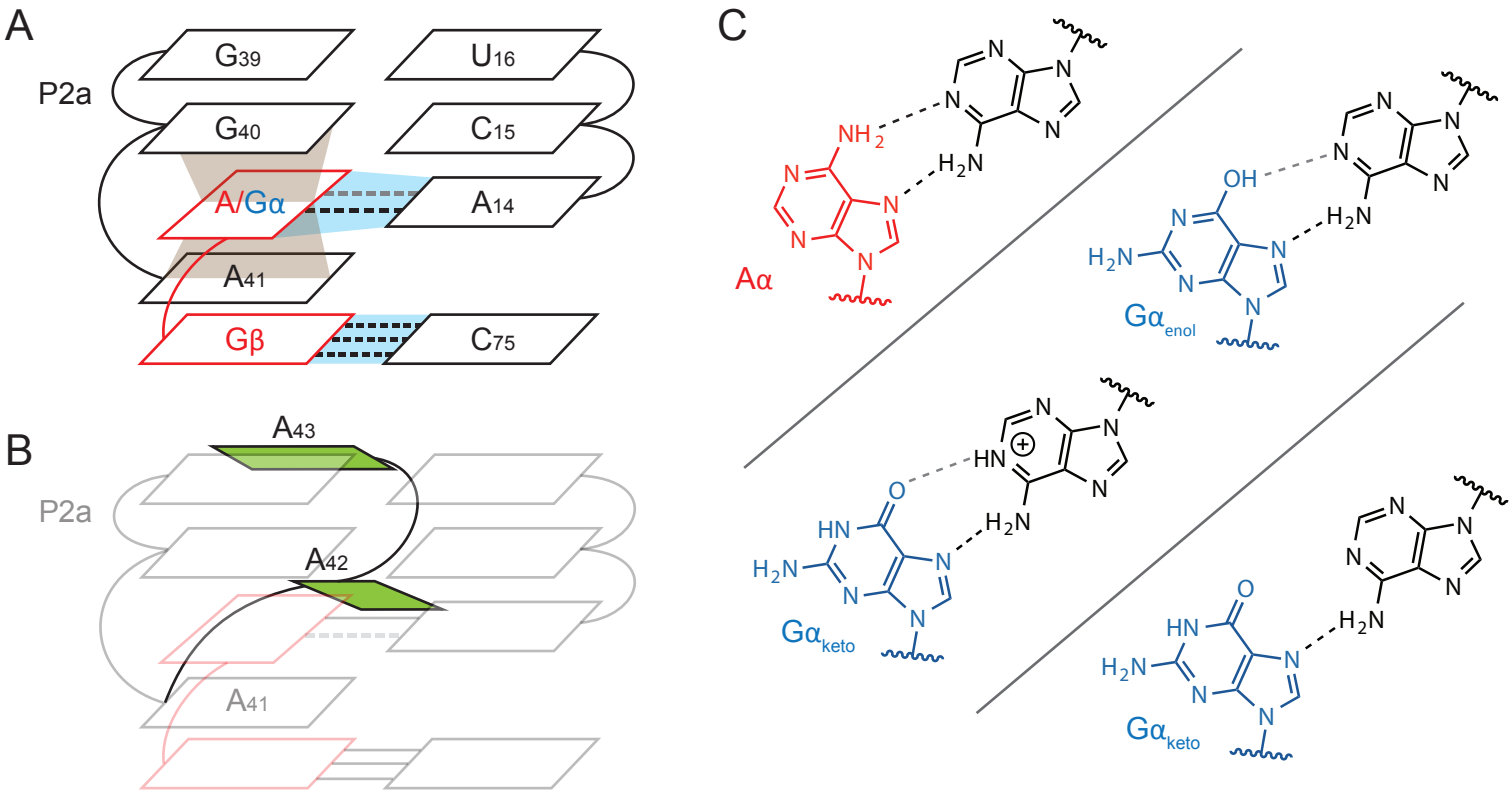
A
P2a
G39
U16
G40
C15
A/Gα
A14
A41
Gβ
C75
B
P2a
A43
A42
A41
C
NH2
H2N
Aα
OH
H2N
Gαenol
HN
O
HN
H2N
Gαketo
H2N
Gαketo

Fig. S5

EXTENDED EXPERIMENTAL PROCEDURES

RNA preparation, purification and complex formation for crystallography

The aptamer domain of the 3',3'-cGAMP riboswitch followed by the hammerhead ribozyme was transcribed *in vitro* using T7 RNA polymerase (Pikovskaya et al. 2009). To facilitate the *in vitro* transcription, a G1-G2 step was introduced instead of the G1-A2 step at the 5'-end of the native riboswitch. In addition, our sequence contained U72-C73 and it was only shown later that the natural riboswitch sequence should be corrected to C72-U73. The transcribed RNA was purified by denaturing polyacrylamide gel electrophoresis (PAGE), followed by anion-exchange chromatography and ethanol precipitation. The complex was generated by annealing the purified 3',3'-cGAMP riboswitch at 70 C with 3',3'-cGAMP or c-di-GMP in a 1:2 molar ratio for 5 min in a buffer containing 100 mM K-acetate, pH 6.8, and 5 mM $MgCl_2$, followed by incubation at 37 C for 5 min and then cooling on ice for 1 h before setting up crystallization trials.

The G20A mutant c-di-GMP riboswitch was transcribed *in vitro* using T7 RNA polymerase similar to the wild-type c-di-GMP riboswitch (Smith et al. 2009). A U1A protein binding RNA loop was also introduced into stem P3 of the G20A mutant to facilitate the crystallization. To improve the crystal resolution, the last G at the 3'-end was removed. The RNA-ligand complex was generated by annealing the purified c-di-GMP riboswitch mutant G20A at 70 C with 3',3'-cGAMP in a 1:2 molar ratio for 5 min in a buffer containing 100 mM K-acetate, pH 6.8, and 5 mM $MgCl_2$ followed by incubation at 37 C for 5 min and then cooling on ice for 1 h. U1A protein in the same buffer was added in a 1:1 molar ratio to the complex and incubated for half an hour before setting up crystallization trials.

Crystallization

The crystals of the aptamer domain of the 3',3'-cGAMP riboswitch with bound 3',3'-cGAMP or c-di-GMP were grown at 20 $^{\circ}$C over a period of 1 week using the sitting-drop vapor diffusion approach after mixing the complex at an equimolar ratio with the reservoir solution containing 0.1 M Na/K-phosphate, pH 6.2-6.6, 0.2 M NaCl and 40-45% PEG400. For data collection, the crystals were quickly flash-frozen in liquid nitrogen.

The crystals of the complex of the G20A mutant c-di-GMP riboswitch with 3',3'-cGAMP were grown from the condition of 0.1 M Na-citrate pH 5.5, 5% PEG1000, 35% iso-propanol over 2 weeks. To collect the x-ray diffraction data, the crystals were transferred to 0.1 M Na-citrate pH 5.5, 5% PEG1000, 35% MPD and quickly flash-frozen in liquid nitrogen.

X-ray data collection and refinement

All the data were collected at 100 K at the NE-CAT beamline ID24C at the Advanced Photon Source, Argonne National Laboratory and processed with XDS programs. The structure of the 3',3'-cGAMP riboswitch bound with 3',3'-cGAMP (space group: $P2_1$) was solved by molecular replacement method based on the structure of c-di-GMP bound to the c-di-GMP Vc2 riboswitch (PDB code: 3IRW) as starting model. The initial RNA model was traced and built in COOT (Emsley and Cowtan, 2004) and refined in PHENIX (Adams et al. 2002). Metal ions and their coordinated waters were identified based on *2Fo-Fc* and *Fo-Fc* maps guided by the coordination geometries. 3',3'-cGAMP molecules were added to the model at the last stage based on the experimental and refined maps, coupled with electrostatic analysis. The structure of the 3',3'-cGAMP riboswitch with bound c-di-GMP (space group: C2) was solved and refined using 3',3'-cGAMP-bound structure as a starting model. The x-ray statistics of the crystals of 3',3'-cGAMP riboswitch with bound 3',3'-cGAMP and with bound c-di-GMP are listed in Table S1.

The structure of the G20A mutant c-di-GMP Vc2 riboswitch with bound 3',3'-cGAMP (space group: $P2_1$) was solved and refined with the structure of the c-di-GMP riboswitch with bound c-di-GMP (PDB code: 3IRW) as starting model. The x-ray statistics of the crystal of G20A mutant c-di-GMP Vc2 riboswitch bound with bound 3',3'-cGAMP are listed in Table S3.

Isothermal titration calorimetry

ITC experiments were performed on a Microcal ITC200 calorimeter at 35 °C. Prior to titration, 0.02-0.04 mM RNA samples were dialyzed overnight at 4 C against an experimental buffer containing 50 mM K-acetate, pH 6.8, 100 mM KCl and 0 to 20 mM

$MgCl_2$. RNAs were refolded by heating at 70 C for 5 min and followed by cooling on ice. 3', 3'-cGAMP, c-di-GMP and other analogs were dissolved in the dialysis buffer at 0.2-0.4 mM concentration and typically titrated into the RNA in the sample cell (V = 207 µL) by 17 serial injections of 2.35 µl each, with a 0.5 µL/s rate, 180 s intervals between injections, and a reference power of 6 µcal/s. The thermograms were integrated and analyzed using the model of one set of sites in Origin 7.0 software (Microcal, Inc.).

Spinach-based fluorescence assays for ligand binding

DNA templates (Table S4) corresponding to riboswitch-Spinach constructs were either purchased as single-stranded oligonucleotides (IDT) or generated via QuikChange site-directed mutagenesis (Agilent Technologies) from a template plasmid following manufacturer instructions. After constructs were confirmed by sequencing, templates were amplified via PCR with primers F and R and the RNA was transcribed *in vitro* using T7 RNA polymerase and purified by denaturing (7.5 M urea) 6% PAGE gel. After elution from the gel, the RNA was precipitated with ethanol, dried, resuspended in water, and the stock concentration was determined by thermal hydrolysis (Wilson et. al. 2014).

Fluorescence activation assays to determine ligand selectivity of different riboswitch-Spinach constructs were performed as previously described (Kellenberger et. al. 2013). Briefly, all assays were performed in 96-well plates (Corning Costar 3915) and analyzed in a SpectraMax Paradigm plate reader (Molecular Devices). RNAs were refolded in binding buffer (40 mM HEPES, 125 mM KCl, and 10 mM $MgCl_2$ at pH 7.5) and added to wells containing binding buffer, 10 µM DFHBI, and ligand at given concentrations or no ligand (control). The reaction plate was incubated at 30˚C in the plate reader and fluorescence measurements were taken over time using 460 nm excitation / 500 nm emission or 448 excitation / 506 nm emission (for Fig. S3 inset). Reported fluorescence values are for reactions that have reached equilibrium and with background fluorescence subtracted, which is defined as fluorescence of buffer without DFHBI.

REFERENCES

Adams, P.D., Grosse-Kunstleve, R.W., Hung, L.W., Loerger, T.R., McCoy, A.J., Moriarty, N.W., Read, R.J., Sacchettini, J.C., Sauter, N.K., and Terwilliger, T.C. (2002). PHENIX: building new software for automated crystallographic structure determination. In Acta Crystallogr D Biol Crystallogr, pp. 1948-1954.

Emsley, P., and Cowtan, K. (2004). Coot: model-building tools for molecular graphics. Acta Crystallogr D Biol Crystallogr *60*, 2126-2132.

Pikovskaya, O., Polonskaia, A., Patel, D. J. and Serganov, A. (2011). Structural princoples of nucleosie selectivity in a 2'-deoxyguanosine riboswitch. Nat. Chem. Biol. *7*, 748-755.

Smith, K.D., Lipchock, S.V., Ames, T.D., Wang, J., Breaker, R.R., and Strobel, S.A. (2009). Structural basis of ligand binding by a c-di-GMP riboswitch. Nat. Struct. Mol. Biol *16*, 1218-1223.

Wilson, S.C., Cohen, D.T., Wang, X.C., and Hammond, M.C. (2014). A neutral pH thermal hydrolysis method for quantification of structured RNAs. RNA *20*, 1153-1160.